Band properties of metallic corundum-phase V_2O_3

1994 J. Phys.: Condens. Matter 6 6477

(http://iopscience.iop.org/0953-8984/6/32/009)

J. Phys.: Condens. Matter 6 (1994) 6477–6484. Printed in the UK

Band properties of metallic corundum-phase V_2O_3

L F Mattheiss
AT&T Bell Laboratories, Murray Hill, NJ 07974, USA

Received 22 March 1994, in final form 16 May 1994

Abstract. Band structure results for metallic corundum-phase V_2O_3 feature narrow (~2.7 eV) t_{2g} conduction bands and a density-of-states peak at E_F such that the heat capacity to band ratio is ~4.4. The predominant V(3d) character of conduction electrons suggests that transport properties will be especially sensitive to cation disorder. It is proposed that the structural and resistivity anomalies that occur in Cr-doped samples may arise from dopants that are interstitial (i.e., at NiAs-type cation sites which are vacant in the corundum structure) rather than substitutional.

As a result of the pioneering studies by McWhan, Rice and Remeika [1] in the late 1960s, vanadium sesquioxide has come to be regarded as the canonical Mott–Hubbard system where the Coulomb interaction between conduction electrons leads to a breakdown of conventional one-electron band theory. Systematic studies [2] have provided details of the temperature, pressure, and composition dependence of the $(V_{1-x}Cr_x)_2O_3$ phase diagram. These include, for example, the boundary parameters that separate the metallic (M), insulating (I), and antiferromagnetic insulator (AFI) regimes. Certainly, the most fascinating consequence of Cr doping is the M–I transition that occurs in a system where long-range order (i.e., the corundum structure) seems to remain unchanged. It should be emphasized that this M–I transition, which is generally described as a Mott transition, is distinct from the M–AFI transition where the metallic corundum structure distorts to form an insulating monoclinic phase [3]. Although the V_2O_3 literature is vast (~500 papers), a review by Mott [4] summarizes the basic issues.

Despite two decades of interest in this material, a reliable picture of the paramagnetic V_2O_3 band structure is still unavailable. The only existing V_2O_3 band-structure results have been derived from simplified tight-binding (TB) treatments [5, 6]. To remedy this situation, a full-potential, scalar-relativistic version [7] of the linear augmented-plane-wave (LAPW) method [8] has been applied to calculate the self-consistent band structure of corundum-phase V_2O_3 [9] in the local-density approximation (LDA). Exchange and correlation effects have been treated using the Wigner interpolation formula [10]. The LAPW basis has included plane waves with a 14.4 Ryd cut-off (~310 LAPWs per formula unit (FU)) and spherical-harmonic terms through $l = 6$ inside the muffin tins. The charge density and potential have been expanded using ~6600 plane waves in the interstitial region and lattice harmonics ($l_{max} = 4$) within the muffin tins. A twenty-two k-point sample in the 1/12 irreducible Brillouin zone (BZ) wedge (see figure 1(b)) has been used to evaluate BZ averages. The atomic $V(3d^4 4s^1)$ and $O(2s^2 2p^4)$ levels have been included as valence electrons in this study, while the remaining inner-shell states are treated via a rigid-core approximation.

The basic features of the corundum structure are shown in figure 1. The circles in figure 1(a) identify the V positions in the non-primitive hexagonal as well as the primitive rhombohedral cell (filled circles). The non-primitive hexagonal (primitive rhombohedral)

0953-8984/94/326477+08$19.50

cell contains six (two) V_2O_3 FU. The cations are visibly displaced from 'ideal' positions where Vs in the hexagonal layers would be coplanar. Each V is octahedrally coordinated by six Os (at distances of ~1.97–2.05 Å); the manner in which these octahedra are linked (via face, edge, and corner sharing) to form a three-dimensional network is illustrated in figure 1(c). The rhombohedral BZ is shown in figure 1(b), along with three zones of the hexagonal supercell (dashed lines).

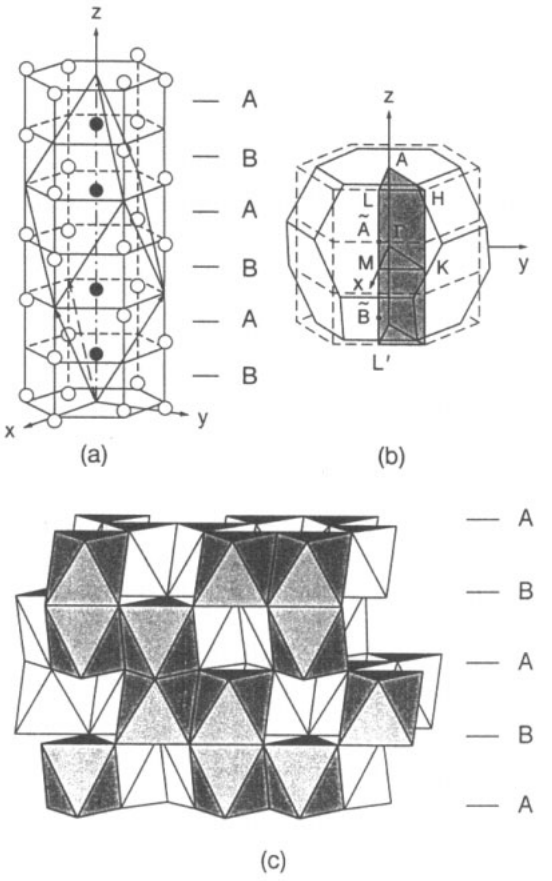

Figure 1. (a) Vanadium-atom positions for corundum-phase V_2O_3 in the primitive rhombohedral (filled circles) and non-primitive hexagonal (circles) cells; (b) rhombohedral Brillouin zone (solid lines) and an equivalent hexagonal-type irreducible wedge; (c) the corundum structure as a linked network of VO_6 octahedra with ordered NiAs-type vacancies.

The corundum structure in figure 1(c) can be derived from a 'parent' NiAs phase by introducing ordered vacancies at 1/3 of the cation sites. This reduces the space-group symmetry from $P6_3/mmc$ to $R\bar{3}c$. Clearly, these vacancies interrupt the c-axis conduction paths that would be available in the NiAs phase where the face-sharing chains of VO_6 octahedra are continuous. The V displacements increase the c-axis V–V bondlengths from ~2.33 Å (for an ideal geometry) to a relaxed value of ~2.70 Å. These relaxations increase the lateral V–V bond distances from ~2.86 to 2.88 Å. An X-atom constituent at a vacancy site would possess nearest-neighbour X–O and X–V bondlengths of ~2.07 and 2.15 Å, respectively.

The present LAPW results for rhombohedral V_2O_3 are plotted in figure 2 along lines on the surface of the hexagonal BZ wedge of figure 1(b). The eighteen low-lying bands originate from the O(2p) states. (Bands are most easily counted along the HA line, where

they are twofold degenerate [11].) The next group of twenty bands represents the V(3d) states. These are split into twelve partially filled t_{2g} subbands (below) and eight empty e_g states (above). The bottom of the V(4s) bands begin at ~4 eV. The reduced symmetry of the corundum structure (i.e., rhombohedral versus hexagonal) causes the bands along L'M and LM to differ. The points labelled $\tilde{A}$ and $\tilde{B}$ in figures 1(b) and 2 correspond to the A and B points on the BZ surface that have been considered earlier [5, 6].

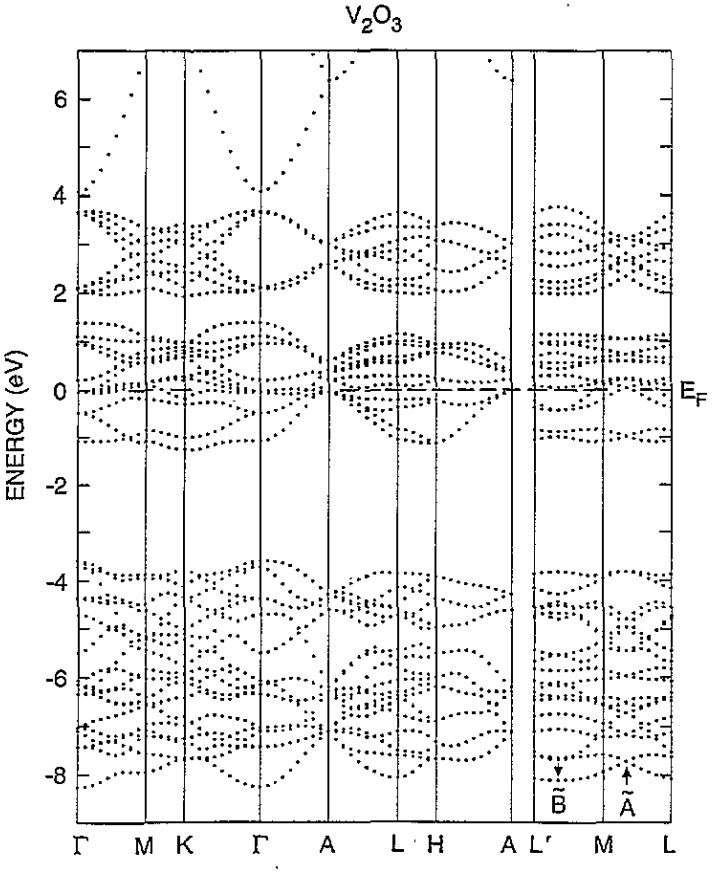

Figure 2. LAPW bands for rhombohedral V_2O_3 along symmetry lines of the hexagonal-type Brillouin zone of figure 1(b).

In contrast to the cuprate high-T_c superconductors where the Cu(3d)–O(2p) orbital energies are nearly degenerate, the V(3d) bands in figure 2 lie several eV above the O(2p) manifold. This is quantified by the V_2O_3 TB parameters that are listed in table 1. The effect of the ~4 eV $\varepsilon_d - \varepsilon_p$ orbital-energy difference is to reduce significantly the extent of p–d hybridization. This is illustrated by the LAPW density-of-states (DOS) results in figure 3. As shown, the V(3d) weight is concentrated primarily in the t_{2g} and e_g manifolds while the O(2p) components dominate the lower energy (~ −4 to −8 eV) regions. Thus, one can conclude that the V(3d) and O(2p) bandwidths in V_2O_3 originate mainly from direct V–V and O–O interactions rather than V–O hybridization. This predominance of V(3d) orbital weight at the Fermi level suggests that transport properties in V_2O_3 will be particularly sensitive to cation disorder.

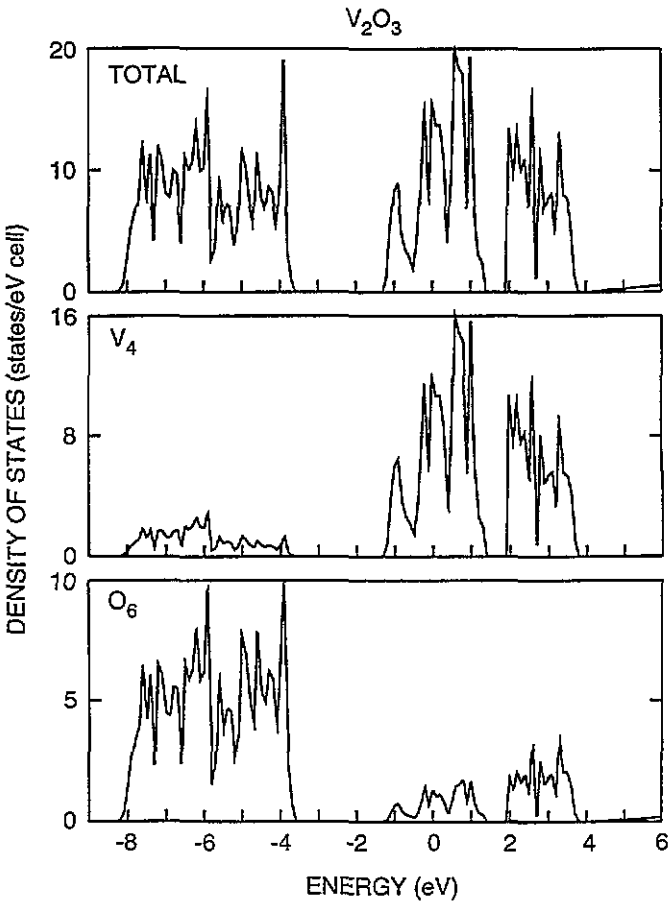

Figure 3. Total and muffin-tin-projected LAPW density-of-states results for rhombohedral V_2O_3.

Table 1. Tight-binding parameters for V_2O_3 (RMS error = 0.2 eV). Parameters in braces {···} have been approximated using simplifying relations (i.e., $(dd\pi) = 0.5|(dd\sigma)|$, etc.) leaving 19 independent parameters.

Site/ interaction	Distance (Å)	Parameters	Value (eV)
V	—	ε_d	−0.33
O	—	ε_s, ε_p	−18.33, −4.49
V–V	2.88	(ddσ), (ddπ), (ddδ)	−0.49, {0.25}, {−0.05}
V–V	2.70	(ddσ), (ddπ), (ddδ)	−0.83, {0.41}, {−0.08}
V–O	2.05	(sdσ), (pdσ), (pdπ)	−2.88, −2.02, 0.87
V–O	1.97	(sdσ), (pdσ), (pdπ)	−1.50, −2.32, 1.14
O–O	2.67	(ssσ), (spσ), (ppσ), (ppπ)	−0.36, {0.52}, 0.74, {−0.37}
O–O	2.95	(ssσ), (spσ), (ppσ), (ppπ)	−0.13, {0.24}, 0.45, {−0.22}
O–O	2.80	(ssσ), (spσ), (ppσ), (ppπ)	−0.24, {0.26}, 0.28, {−0.14}
O–O	2.89	(ssσ), (spσ), (ppσ), (ppπ)	−0.12, {0.18}, 0.29, {−0.15}

The calculated value for the V_2O_3 DOS at E_F is $N(E_F) = 15.5$ states eV^{-1}/cell, or ~1.94 states eV^{-1}/(spin V atom). As a result, the ratio of the measured [12] specific-heat DOS (N_γ

= 8.5 states eV^{-1}/(spin V atom)) to the band value is ~4.4. Since the present DOS calculation utilizes a fairly coarse (~70 *k* points) BZ mesh in combination with tetrahedral interpolation, some fine-structure details may be averaged out in these results. Also, the measured DOS value has been derived from a Ti-doped sample; model results presented below suggest that doping can alter the intrinsic DOS to an extent that the measured specific-heat N_γ values may differ significantly from that of a perfect V_2O_3 sample.

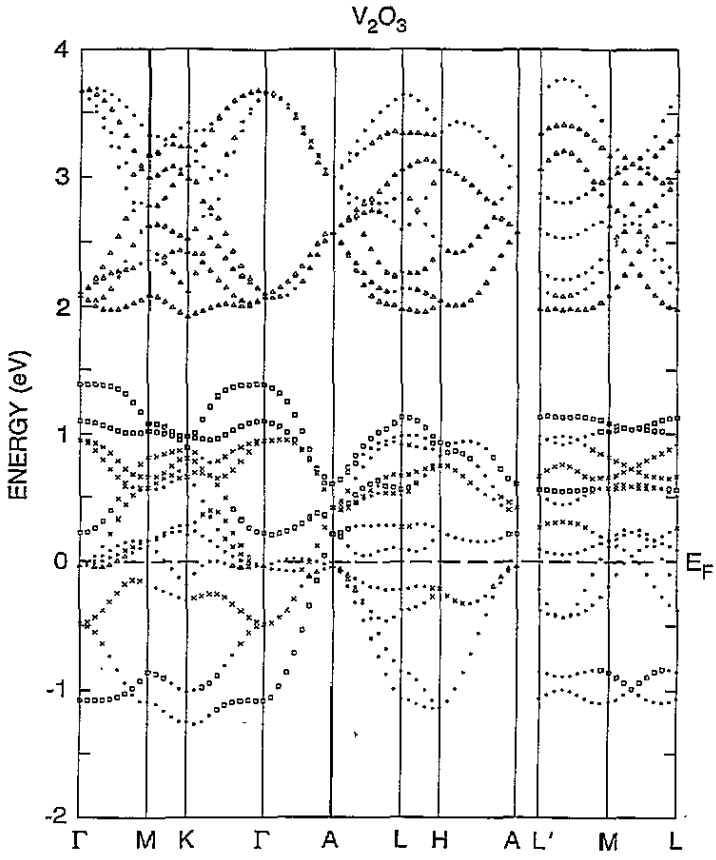

Figure 4. Expanded view of the V(3d) bands, including the lower t_{2g} and upper e_g manifolds. Distinctive symbols identify bands containing at least 40% $d_{3z^2-r^2}$ (squares), d_{xy,x^2-y^2} (crosses), or $d_{xz,yz}$ (triangles) orbital weight within the vanadium muffin tins.

A close-up view of the V(3d) bands near E_F is shown in figure 4, where the previous results are replotted with an expanded energy scale. Here, distinctive symbols have been added to identify the predominant orbital character of individual bands. The squares and crosses show that the partially filled t_{2g} bands [13] involve $d_{3z^2-r^2}$ and d_{xy,x^2-y^2} orbitals that form π-type bonds with neighbouring oxygens while the upper e_g manifold consists mainly of σ-bonding $d_{xz,yz}$ states. These orbital characteristics are also reflected in the V(3d)-projected DOS results in figure 5. The $d_{3z^2-r^2}$ orbital weight is confined primarily to the lower t_{2g} subbands. However, the fact that the d_{xy,x^2-y^2} and $d_{xz,yz}$ states transform according to the same irreducible representation [11] of the V-site point group causes significant intermixing between the t_{2g} (d_{xy,x^2-y^2}) and e_g ($d_{xz,yz}$) components.

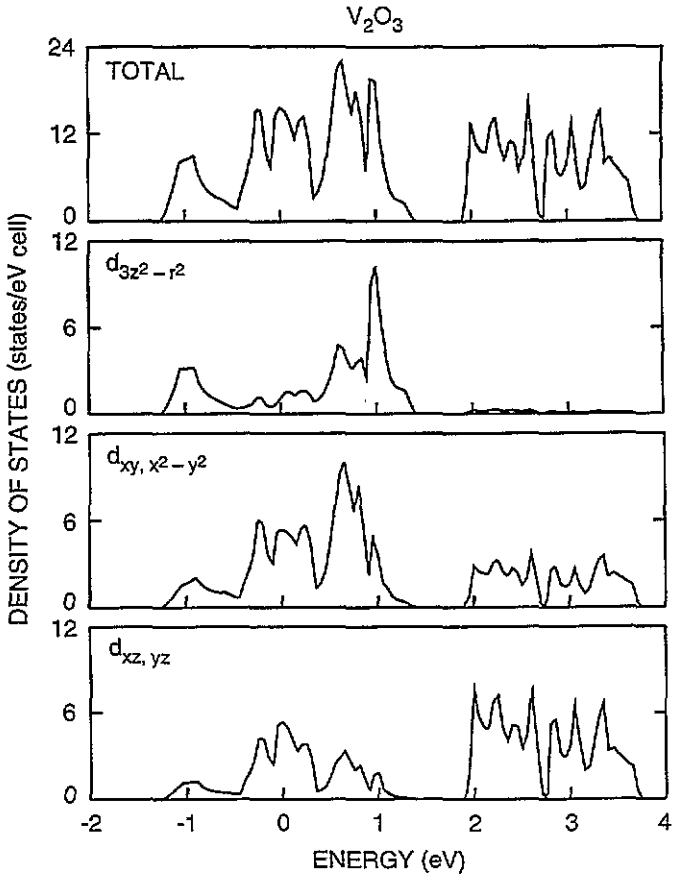

Figure 5. Total and V(3d)-projected density-of-states results for V_2O_3, including separate t_{2g} ($d_{3z^2-r^2}$, $d_{xy,\,x^2-y^2}$) and e_g ($d_{xz,\,yz}$) components.

Since the calculated V_2O_3 band properties appear to be quite normal and exhibit no obvious signs of an impending electronic instability, it is reasonable to explore alternative explanations for the M–I transition in this system. I propose that the transport [14] and structural [15] anomalies that are observed in Cr-doped $(V_{1-x}Cr_x)_2O_3$ samples with $x = 0.01$ are due in fact to cation disorder. Previously, it has been assumed implicitly that Cr doping is substitutional. If Cr occupied the 'vacancy' sites of the parent NiAs structure, then the resulting defect-induced scattering could well dominate the transport properties of such materials. This might allow one to explain, for example, the fact that ~1% Cr doping increases the residual resistivity by an amount that is ten times greater than expectations [14]. It may also account for the observation [15] of two distinct (α and β) corundum-type $(Cr_{0.01}V_{0.99})_2O_3$ phases with slightly different lattice parameters. Obviously, the actual location of Cr dopants is an important issue that should be investigated by site-sensitive techniques (such as ion channelling and extended x-ray absorption fine structure etc).

Although the occurrence of Cr interstitials may be favoured because of its smaller ionic size, V constituents may also form interstitial defects in undoped samples, particularly at higher temperatures where the lattice is expanding. This may explain, for example, the fact that high-temperature (~500 K) NMR data exhibit line-shape changes in pure V_2O_3

that extend over 12-hour periods [16]. This has led to the observation 'that the kinetics of the M–I phase transition in pure V_2O_3 is slow'. It is noted that this 'sluggishness' may be due to thermally induced tunnelling of Vs through the shared octahedral faces that separate neighbouring corundum and vacancy sites in figure 1(c) until thermal equilibrium is reached.

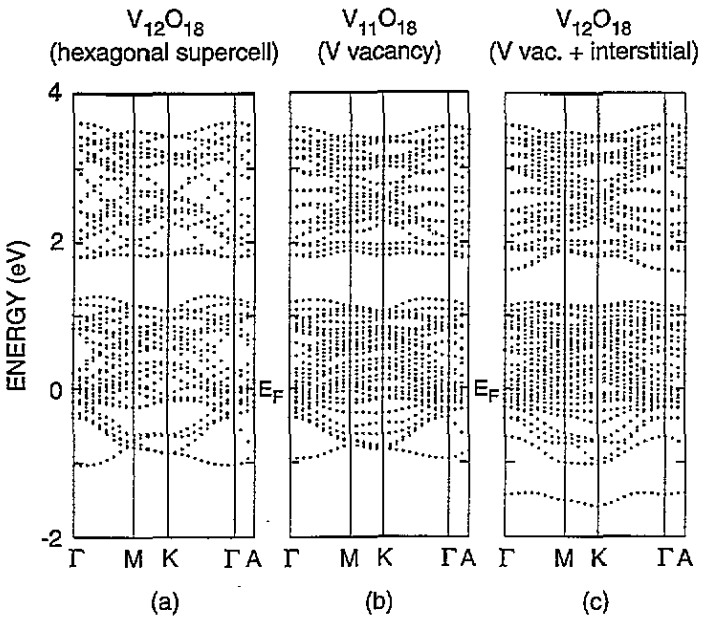

Figure 6. Tight-binding results for (a) a hexagonal $V_{12}O_{18}$ supercell, (b) a vacancy-ordered $V_{11}O_{18}$ superlattice, and (c) a model paired-defect $V_{12}O_{18}$ supercell containing one (corundum-type) vacancy and one (NiAs-type) interstitial at neighbouring *c*-axis sites in figure 1(a).

Realistic estimates of the effect of V vacancies and vacancy-interstitial pairs on the V_2O_3 band structure have been derived from simple TB studies. The results are summarized in figure 6 where folded $V_{12}O_{18}$ hexagonal-supercell TB bands (figure 6(a)) are compared with those for model structures containing either ~17% ordered V vacancies (figure 6(b)) or ~17% vacancy–interstitial pairs (figure 6(c)). The vacancy–interstitial perturbation is especially strong, causing one t_{2g} level to be pushed upward (to a band energy at Γ of ~1.96 eV) into the lower portion of the e_g subbands. The effect of such defects on the electronic properties of perfect materials is illustrated further by considering the DOS. It is found that, while the DOS (per V atom) at E_F for the $V_{11}O_{18}$ results in figure 6(b) is increased by 40% over the reference $V_{12}O_{18}$ results (figure 6(a)), the corresponding vacancy–interstitial $V_{12}O_{18}$ bands in figure 6(c) yield a value that is diminished by 30%. One can conclude from these model studies that such defects can alter significantly the transport and thermodynamic properties of corundum-phase V_2O_3.

In summary, the calculated LDA band properties of metallic V_2O_3 exhibit sharp DOS structure and predominant V(3d) character near E_F. It is proposed that the structural and resistivity anomalies that are widely attributed a Mott transition in V_2O_3 may arise instead from 'interstitial' defects where V or (intended substitutional) dopants occupy NiAs-type rather than corundum sites. It is suggested that site-sensitive techniques be applied to both stoichiometric and doped V_2O_3 samples in order to resolve these important structural issues.

Acknowledgments

I am pleased to acknowledge useful conservations with S A Carter, D R Hamann, A J Millis, D W Murphy and G A Thomas on the subject of this investigation.

References

[1] McWhan D B, Rice T M and Remeika J P 1969 *Phys. Rev. Lett.* **23** 1384
[2] McWhan D B and Remeika J P 1970 *Phys. Rev.* B **2** 3734
[3] Demier P D and Marezio M 1970 *Phys. Rev.* B **2** 3771
[4] Mott N F 1990 *Metal–Insulator Transitions* 2nd edn (London: Taylor & Francis)
[5] Nebenzahl I and Weger M 1971 *Phil. Mag.* **24** 1119
[6] Ashkenazi J and Chuchem T 1975 *Phil. Mag.* **32** 763
[7] Mattheiss L F and Hamann D R 1986 *Phys. Rev.* B **33** 823
[8] Andersen O K 1975 *Phys. Rev.* B **12** 3060
[9] Demier P D 1970 *J. Phys. Chem. Solids* **31** 2569
[10] Wigner E 1934 *Phys. Rev.* **46** 1002
[11] Cracknell A P, Davies B L, Miller S C and Love W F 1979 *Kronecker Product Tables* vol 1 (New York: Plenum)
[12] McWhan D B, Remeika J P, Rice T M, Brinkman W F, Maita J P and Menth A 1971 *Phys. Rev. Lett.* **27** 941
[13] The two lowest t_{2g} conduction bands are entirely filled, while bands 3–7 are partially occupied. In particular, there are 0.002 and 0.171 holes/cell in bands 3 and 4, respectively (i.e., $h_3 = 0.002$, $h_4 = 0.171$) and compensating electrons in bands 5–7 (i.e., $e_5 = 0.166$, $e_6 = 0.006$, $e_7 = 0.001$).
[14] McWhan D B, Menth A, Remeika J P, Brinkman W F and Rice T M 1973 *Phys. Rev.* B **7** 1920
[15] Robinson W R 1975 *Acta Crystallogr.* B **31** 1153
[16] Kerlin A L, Nagasawa H and Jerome D 1973 *Solid State Commun.* **13** 1125